J Mater Sci: Mater Electron (2021) 32:28051–28064

Co-precipitation synthesis of reusable ZnAl-CLDH/ZIF-8 heterojunction for enhanced photodegradation of organic dye

Yinke Wang[1], Yijian Zheng[1], Guoqing Zhao[1], Shichao Liu[1], Jun Hu[1], Xinqi Long[1], Zixin Xiao[1], Hang Zhang[2], and Feipeng Jiao[1,*]

[1] School of Chemistry and Chemical Engineering, Central South University, Changsha 410083, People's Republic of China
[2] Jiangsu World Top Thermal Technology Co., Ltd, Huai'an 211699, People's Republic of China

Received: 20 July 2021
Accepted: 26 September 2021
Published online: 25 October 2021

ABSTRACT

The ZnAl calcined layered double hydroxides/ZIF-8 composites (ZnAl-CLDH/ZIF-8) were successfully synthesized by a simple and efficient co-precipitation method. Characterizations including XRD, SEM, XPS, UV–vis DRS and EIS were used to investigate the structures and the morphologies of the fabricated photocatalysts. Furthermore, the photocatalytic properties of the composites were evaluated by the photodegradation of Methyl blue (MB) under irradiation. The catalyst showed a high efficiency (97.35%) at the mass ratio of ZIF-8 was 5%. It is worth mentioning that the removal efficiency of MB is still higher than 90% for reused ZnAl-CLDH/ZIF-8 after five cycle runs, confirming the promising practical application. Based on the experimental results, a possible mechanism of decomposition of MB by the ZnAl-CLDH/ZIF-8 heterojunction was proposed.

1 Introduction

In recent decades, as promising materials in the fields of new energy, environmental protection, and green economy, semiconductor photocatalysts with unique optical and electrical properties have received extensive attention from scholars in terms of sustainable development [1–5]. Layered double hydroxides (LDHs), as an inorganic layered semiconductor with special structure, can be synthesized by some simple methods [6–8]. LDHs has been widely investigated in many fields such as electrochemistry, adsorption, polymerisation, catalysis and biology. Thus, LDHs is considered to be one of the important promising clay materials [7, 8]. The formula of LDHs can be expressed by $[M^{2+}_{1-x}M^{3+}_{x}(OH)_2]^{x+}[A^{n-}_{x/n}]\cdot mH_2O$, where M^{2+} and M^{3+} represent divalent (Mg^{2+}, Zn^{2+}, or Ni^{2+}) and trivalent metal cations (Ga^{3+}, Fe^{3+}, or Mn^{3+}), respectively [4, 7]. The value of x is equal to $M^{3+}/(M^{2+} + M^{3+})$. Besides, A^{n-} is an anion, such as CO_3^{2-}, SO_4^{2-} and Cl^- [9–11]. LDHs have been widely studied in the use of catalysts, CO_2 absorbents, electrode and ion exchange carriers because of its several advantages [2, 7]. Considered to

Address correspondence to E-mail: jiaofp@csu.edu.cn; jiaofp@163.com

https://doi.org/10.1007/s10854-021-07118-4

be a replacement of TiO_2-based photocatalyst, LDHs not only has a large specific surface area and acid–base resistance, but also has low raw material costs and easy-adjust composition [9–13]. Furthermore, LDH would be converted into CLDH after calcination at a high temperature. According to previous reports, CLDH has larger adsorption capacity, higher catalytic activity and better thermal stability than LDH because of the formation of metal oxide nanocrystals [2, 6, 13]. Wu et al. [13] fabricated a Cu_2O/ZnAl-CLDH photocatalyst for the removal of methyl orange (MO). When the calcination temperature is 500 °C and the initial concentration of MO is 20 mg/L, the photocatalytic efficiency reached 90.18% under visible light irradiation. After three cycles, the degradation ratio is still higher than 80%. Liu et al. [6] synthesized CLDH/$FeWO_4$ heterojunctions by a biotemplate. This catalyst showed both large adsorption capacity and high photocatalytic activity toward Congo Red (CR). However, because of the narrow band gap of the individual CLDH, it usually has few generation of photogenerated carriers and fast recombination of hole-electron pair. Therefore, combining with another class of materials with a wider band gap could be a simple approach to improve the photocatalytic activity [2, 6, 14].

Metal–organic frameworks (MOFs), as a kind of coordination polymers with porous structure, are normally formed by self-assembled metal ions or clusters and organic ligands [15–20]. In recent years, MOFs have shown great application potential in various field because of some special advantages, such as large specific area, low density, adjustable structure and high stability [16–18]. In the field of photocatalysis, MOFs can be used as catalysts because the photogenerated electrons can be transferred to the metal centers [15–17]. As a typical class of MOFs, Zeolitic imidazolate frameworks (ZIFs) are composed of bivalent metal cations and imidazole ligands [17–20]. Due to its thermal and chemical stability, as well as rapid and simple synthetic method, ZIF-8, whose metal ion is Zn^{2+}, has received great attention by researchers in the photocatalysis field. Besides, ZIF-8 has a wide band gap (> 4.0 eV) which is favorable for the generation and separation of photogenic carriers. Meanwhile, the energy band structure limits its practical application because of its low light utilization [21–23]. Therefore, CLDH and ZIF-8 can complement the advantages of each other to produce new composite materials with good optical and catalytic properties.

In this work, a simple co-precipitation method was used to fabricate ZnAl-CLDH/ZIF-8 composites. As far as we know, it is the first time that ZnAl-CLDH and ZIF-8 have been combined and used for photodegradation. Under the light irradiation, the photocatalytic activities of the as-prepared samples were investigated by the decomposition of MB as a kind of simulated organic pollutants. Furthermore, the morphology and structural characteristics of the samples were analyzed by some characterizations. In addition, through investigating the band structures of the catalysts and the results of radical scavenging test, the possible mechanism of dye degradation by the ZnAl-CLDH/ZIF-8 heterojunction was proposed.

2 Experimental

2.1 Materials

$Zn(NO_3)_2{\cdot}6H_2O$ and $Al(NO_3)_3{\cdot}9H_2O$ was obtained from Tianjin Kemiou Chemical Reagent Co., Ltd. and Xilong chemical Co., Ltd., respectively. 2-methylimidazole was purchased from Shanghai Titan Scientific Co., Ltd. MB was acquired from Tianjin Hengxing Chemical Reagent Manufacturing Co., Ltd. Ethylene glycol was bought from Sinopharm Chemical Reagent Co., Ltd. (China). The purity of all reagents was analytical grade. Furthermore, in this work, they were used without any purification. The deionized water was used throughout the experiment.

2.2 Preparation of ZnAl-LDH

According to typical literature methods, co-precipitation was used to prepare the ZnAl-LDH [6, 14, 24–26]. Solution A was made by mixing $Zn(NO_3)_2{\cdot}6H_2O$ and $Al(NO_3)_3{\cdot}9H_2O$ in 50 mL deionized water and the initial molar ratio of Zn/Al was equal to 2. Meanwhile, containing NaOH and Na_2CO_3, solution B was prepared with deionized water to control the pH value (pH = 9.0) in the reaction. Then, solution B was dropped into A slowly under stirring until pH reached the expected value. After stirring continuously at room temperature for a period of time, the obtained suspension was crystallized at 60 °C for one day, which was followed by washing and filtration. Finally, the precipitate can be

collected by desiccation at 60 °C in a vacuum oven for several hours.

2.3 Preparation of ZnAl-CLDH

In order to obtain the ZnAl-CLDH, the ZnAl-LDH sample was calcined in a muffle furnace at 500 °C for 4 h, then the powders were collected [26].

2.4 Synthesis of ZnAl-CLDH/ZIF-8

ZnAl-CLDH/ZIF-8 composites were fabricated by a co-precipitation method. Firstly, different masses of ZnAl-CLDH (4.3240 g, 2.0482 g, 1.2896 g, 0.9103 g) and 1 mmol (0.2975 g) $Zn(NO_3)_2{\cdot}6H_2O$ were uniformly dispersed in 50 mL methanol to form solution C with stirring for 1 h. Meanwhile, 4 mmol (0.3284 g) 2-methylimidazole was also dissolved in 50 mL methanol to form solution D. Then, solution D was added into C slowly and the new solution was stirred for 3 h. Finally, the white sediments can be separated from the slurry by centrifugation, washed with methanol and desiccation at 60 °C for 24 h. The fabricated products with different mass ratio of ZIF-8 (5%, 10%, 15%, 20%) were marked as CZ-5, CZ-10, CZ-15, and CZ-20, respectively. For comparison, pure ZIF-8 was also synthesized through the same method without ZnAl-CLDH.

2.5 Characterization of samples

The crystalline phases of the prepared composites were analyzed by XRD patterns (Bruker D8 Advance X-ray diffractometer with Cu-Kα radiation (1.5406 Å)). The SEM (TESCAN MIRA3 LMU) instrument was used to explore the morphologies and microstructures of the samplesat an acceleration voltage of 10 kV. The BET (Brunauer–Emmett–Teller) surface areas analysis was carried out using the N_2 adsorption–desorption analyzer (77.3 K, 6 h outgas, and 150 °C in advance treatment) at liquid nitrogen temperature (− 196 °C). The XPS measurements were performed by the ULVAC-PHI spectrometer with Al K_α radiation (1486.6 eV) at 3.0 × 10^{-10} mbar. Furthermore, the XPS data was fitted by XPSPEAK 41 (software) through adjusting the Lorentzian–Gaussian proportion of the Voight function. The UV–visible diffuse reflection spectroscopy (UV–vis DRS) were implemented on a spectrophotometer (Schimadzu 2401 spectrophotometer).

2.6 Photocatalytic test

A certain amount of photocatalysts (50 mg) was added into 50 mL Methylene blue (MB) solution (10 ppm) to ensure that the catalyst concentration was 1 g/L. After stirring in the dark for 30 min to reach the adsorption–desorption equilibrium, the mixture was exposed to a visible light by a 500 W mercury lamp. During the irradiation process, 3 mL solution was collected every 15 min after filtering to remove the catalyst. Finally, the UV–Vis spectrophotometer was used to measure the absorbance of the solution at 664 nm and investigate the concentration of MB.

According to the Beer-Lambert law, the concentration of MB is linearly to the absorbance [7, 12, 21, 25]. Therefore, the photocatalytic efficiency can be evaluated by the following formula: $(C_0 - C_t)/C_0 \times 100\%$, where C_0 is the initial concentration of MB and C_t is the concentration at time t.

3 Results and discussion

3.1 Characterization of photocatalysts

3.1.1 XRD

Figure 1 exhibits the XRD patterns of all as-prepared samples. The device of ZnAl-LDH shows the characteristic reflection peaks at 2θ = 11.6°, 23.4°, 34.6°, 39.1°, 46.6°, 60.2° and 61.5°, corresponding to (003), (006), (012), (015), (018), (110) and (113) planes of the typical LDH material (JCPDS No. 38-0486)

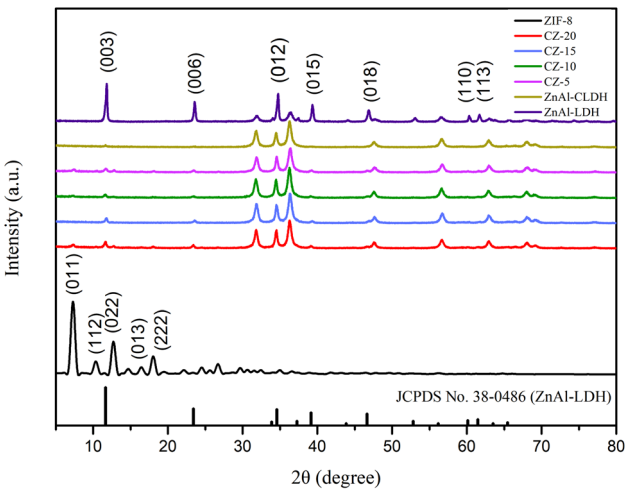

Fig. 1 The XRD patterns of photocatalysts

[2, 7, 24–26]. After calcination, the characteristic peaks of LDH are disappeared and the diffraction reflections of ZnO can be observed (JCPDS No. 36-1451) [14, 27, 28]. According to the previous reports, the pattern of pure ZIF-8 in Fig. 1 displays the strong reflections of (011), (112), (022), (013) and (222) at $2\theta = 7.4°$, 12.8°, 14.8°, 16.5° and 18.1° respectively, which demonstrates a high crystallinity of the prepared ZIF-8 [23, 28–32]. The XRD patterns of ZnAl-CLDH/ZIF-8 composites contain the characteristic peaks of two single materials. However, compared with ZnAl-CLDH, the peak intensities of ZIF-8 are weaker due to the low content of ZIF-8. On the contrary, the diffraction peaks of ZnAl-CLDH are clearly shown in the XRD patterns of the composites, indicating the crystallinity of CLDH was not changed by the addition of ZIF-8.

3.1.2 SEM

The SEM images were used to observe the morphologies of ZnAl-LDH, ZnAl-CLDH, ZIF-8 and ZnAl-CLDH/ZIF-8 composites. As shown in Fig. 2a, the layered structure with a certain aggregation can be observed, indicating the successful preparation of LDH [3, 33–35]. Then, a part of the layered structure was collapsed and smaller particles were produced after calcining (Fig. 2b). Therefore, the surface area could be increased [13, 27]. Large specific surface area increases the contact surface with the reaction substrate, which is conducive to the photodegradation process. Figure 2c shows the SEM image of pure ZIF-8, which demonstrates the dodecahedron structure [30, 36–39]. This type of structure has a large specific surface area to enhance the adsorptive property of the composites [21, 29, 39]. Obviously, the morphology of ZnAl-CLDH/ZIF-8 composite is similar to that of ZnAl-CLDH (Fig. 2d), which indicates a negligible change in the structure of ZnAl-CLDH with the incorporation of a small amount of ZIF-8. Furthermore, the denser particles were loaded on the uncollapsed nanosheets, proving the successful combination of the two materials.

Furthermore, the elements types and contents were investigated by EDX (energy-dispersive X-ray spectroscopy). As shown in Fig. 2e, Zn (31.35%), Al (6.62%), O (41.05%), C (20.31%) and N (0.67%) exist in the composite. The content of zinc is high because both ZnAl-CLDH and ZIF-8 contain zinc. The characteristic peaks of Al and N are attributed to ZnAl-CLDH and ZIF-8, respectively. The EDX results can prove the coexistence of ZnAl-CLDH and ZIF-8 and accord with XRD and SEM analysis.

3.1.3 XPS

The chemical status of ZnAl-CLDH/ZIF-8 composite was investigated by XPS. As seen in Fig. 3a, the presence of Zn, Al, O and C elements proves the successful synthesis of the composite, which is consistent with the XRD results. Based on Fig. 3b, the characteristic peaks of Zn 2p are located in 1021.55 eV and 1044.82 eV, which are responsible for Zn 2p3/2 and Zn 2p1/2, respectively [11, 13, 33]. Meanwhile, Fig. 3c shows the binding energy of Al 2p at 73.93 eV, which is related to ZnAl-CLDH [6, 7, 24]. The binding energies of O 1 s core level centered at 530.61 eV and 531.48 eV, corresponding to Fe–O and O–H and Zn–O [19, 20, 25, 40]. The spectrum of C 1 s can be divided into two parts at 284.83 eV and 288.63 eV, which are responsible to the non-oxygenated ring C (C–C) and the carboxylate carbon (O–C=O) respectively [36, 39].

3.1.4 UV–vis DRS

The optical absorption spectra of the obtained ZnAl-LDH, ZnAl-CLDH, ZIF-8 and ZnAl-CLDH/ZIF-8 were demonstrated in Fig. 4a. Obviously, all the responses of them occurred in the ultraviolet region (200–400 nm). Furthermore, although the spectrum of ZIF-8 shows an adsorption edge at 221 nm, the characteristic light absorption edge of ZnAl-CLDH/ZIF-8 composite is almost the same as that of ZnAl-CLDH (295 nm), which is due to the low mass ratio of ZIF-8 in the composite. However, the increase of absorbance indicates that the addition of ZIF-8 greatly improves the intensity of light absorption. Calculated by Kubelka–Munk function [8–14, 34–39, 41, 42], the bandgaps (E_g) of the as-prepared samples were shown in Fig. 4b–e. The $h\nu$ and $(Ah\nu)^2$ were taken as the X-axis and the Y-axis respectively because the samples were indirect gap semiconductors. After calcined, the E_g of ZnAl-CLDH (2.42 eV) is a little narrower than that of ZnAl-LDH (2.48 eV). In addition, the incorporation of ZIF-8 with a wide bandgap (4.18 eV) leads the bandgap of the composite wider (2.53 eV). Therefore, the ZnAl-CLDH/ZIF-8 shows an optimal optical properties among these four samples.

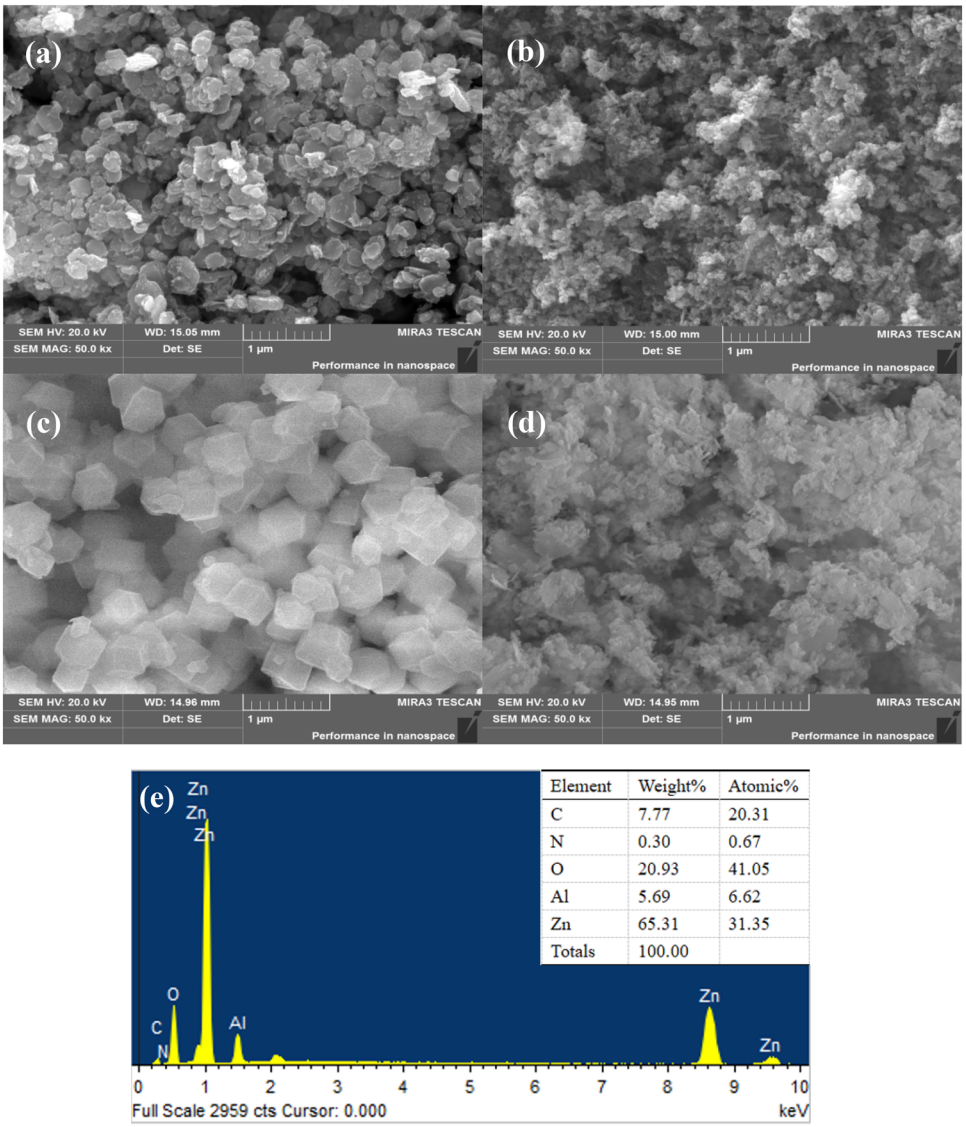

Fig. 2 SEM images of **a** ZnAl-LDH, **b** ZnAl-CLDH, **c** ZIF-8, **d** ZnAl-CLDH/ZIF-8, **e** EDX energy spectra of ZnAl-CLDH/ZIF-8

3.1.5 EIS

The electrochemical impedance spectroscopy (EIS) of the as-prepared samples was investigated by Nyquist plots at open circuit voltage (Fig. 5), displaying the varied charge-transfer resistance (R_{CT}) in ZnAl-CLDH, ZIF-8 and ZnAl-CLDH/ZIF-8 composite [42, 43]. As the measured impedance was mainly affected by electrolyte resistance and charge transfer resistance, a simple electrical equivalent circuit shown in Fig. 5 was used to fit the EIS data [13]. Figure 5 clearly reveals that the diameter of the semicircle arc of the ZnAl-CLDH/ZIF-8 composite is the smallest among all the three samples, confirming that the ZnAl-CLDH/ZIF-8 shows the lowest R_{CT}. The specific parameters were provided in Table 1. The charge-transfer resistance is closely related to the electron transfer efficiency, which affects the photocatalytic activity of the photocatalyst. Therefore, compared with ZnAl-CLDH and ZIF-8, ZnAl-CLDH demonstrates a optimal electron transfer efficiency, indicating that a faster transfer rate of photogenerated electrons and holes, which is conducive to the separation of photogenerated carriers.

3.1.6 BET

The N_2 adsorption test was carried out to investigate the physico-chemical properties of the prepared samples. As type IV isotherms with type H3 hysteresis loops, the N_2 adsorption–desorption isotherms of ZnAl-CLDH, ZIF-8 and CZ-5 were

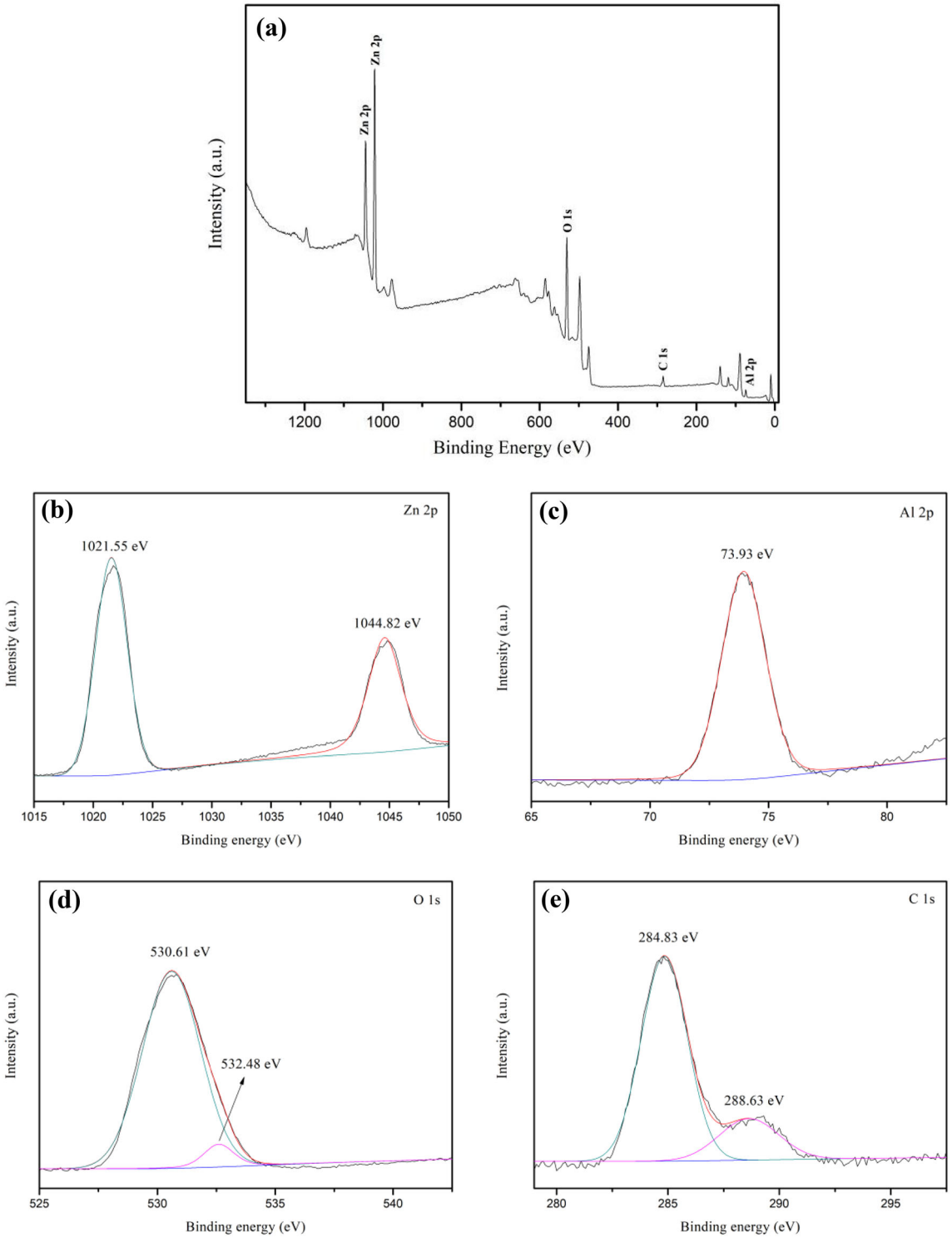

Fig. 3 XPS spectra of ZnAl-CLDH/ZIF-8: **a** Survey spectra, **b** Zn 2p, **c** Al 2p, **d** O 1 s, and **e** C 1 s

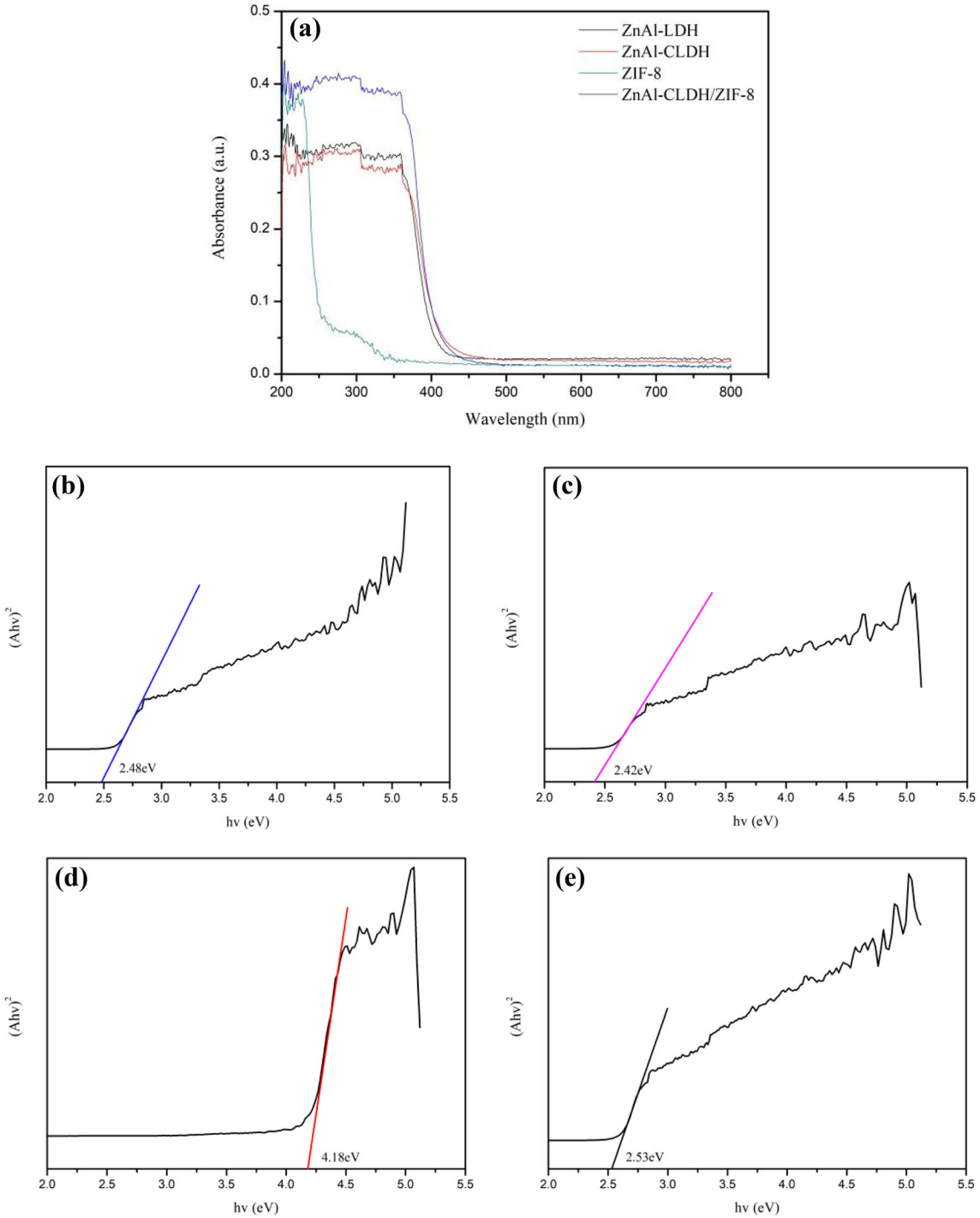

Fig. 4 **a** UV–vis DRS of prepared samples; Energy bandgaps of **b** ZnAl-LDH, **c** ZnAl-CLDH, **d** ZIF-8 and **e** ZnAl-CLDH/ZIF-8

demonstrated in Fig. 6a. Furthermore, the curves shift to a higher relative pressure approaching $P/P_0 = 1$, indicating that these samples were mesoporous materials with some macropores larger than 50 nm in diameter. These results were further confirmed by the Barret–Joyner–Halenda (BJH) pore size distributions in Fig. 6b. The specific physico-chemical parameters were listed in Table 2. The surface area of ZnAl-CLDH was improved from 34.377 m^3/g to 63.193 m^3/g after coupling 5% wt ZIF-8. Therefore, more active sites would be exposed on the surface of

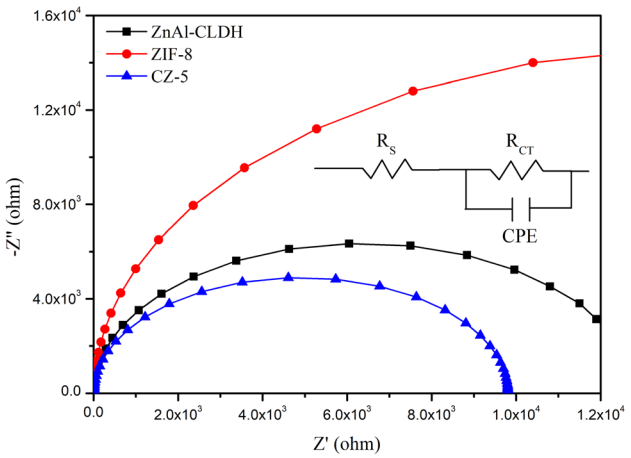

Fig. 5 EIS of ZnAl-CLDH, ZIF-8 and ZnAl-CLDH/ZIF-8

Table 1 EIS parameters for different samples

Samples	R_s (Ω cm^2)	R_{CT} (Ω cm^2)	Q_C (F cm^2)
ZnAl-CLDH	9.192	1.27e^4	2.625e^{-5}
ZIF-8	14.58	2.921e^4	5.825e^{-6}
CZ-5	10.86	0.9795e^4	2.175e^{-6}

the catalyst, which could improve the adsorption capacity and photocatalytic performance.

3.2 Photocatalytic activities of catalysts

3.2.1 *Effect of various photocatalysts*

The photocatalytic activities of fabricated ZnAl-CLDH photocatalysts with different loading of ZIF-8 are investigated by photodegradation of MB solution under light irradiation. For comparison, pure ZnAl-LDH, ZnAl-CLDH and ZIF-8 were placed at the same condition to evaluate the properties. Before irradiation, the as-prepared samples were stirred in the dark for 30 min to achieve the adsorption–desorption equilibrium. The photodegradation rates are indicated by C_t/C_0, where C_t and C_0 are the real time concentration in the degradation process and the initial MB concentration (10 mg/L) respectively, and the results are shown in Fig. 7a. After calcination, ZnAl-CLDH shows the better property than ZnAl-LDH. The photocatalytic rate of CZ-5 (5% ZIF-8) reached 97.35% in 135 min, which is higher than that of pure ZnAl-CLDH and ZIF-8, proving the

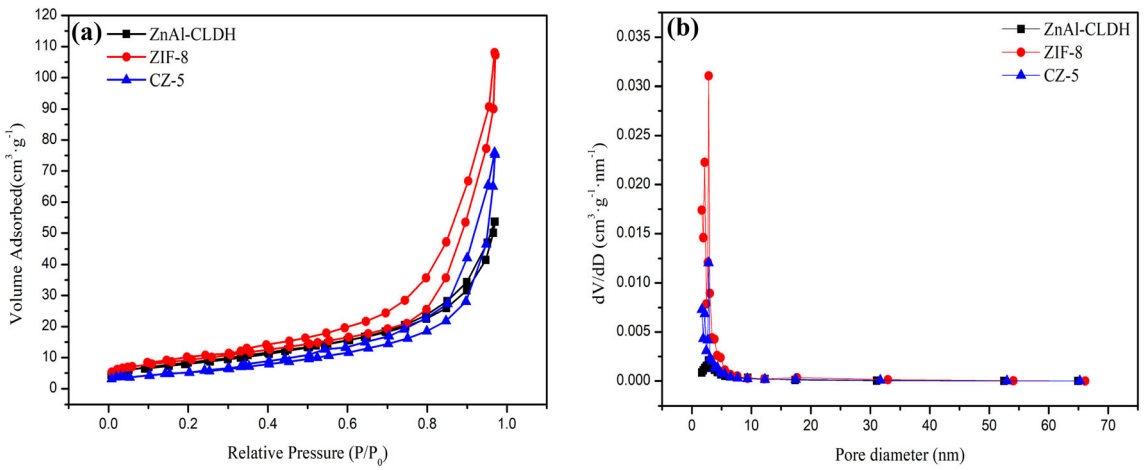

Fig. 6 **a** Nitrogen adsorption isotherms and **b** Pore size distribution curves of ZnAl-CLDH, ZIF-8 and ZnAl-CLDH/ZIF-8

Table 2 The physico-chemical properties of the samples

Catalyst	Pore diameter (nm)	Pore volume (cc/g)	Surface area (m^3/g)
ZnAl-CLDH	2.802	0.085	34.377
ZIF-8	2.821	0.294	159.507
CZ-5	2.806	0.146	63.193

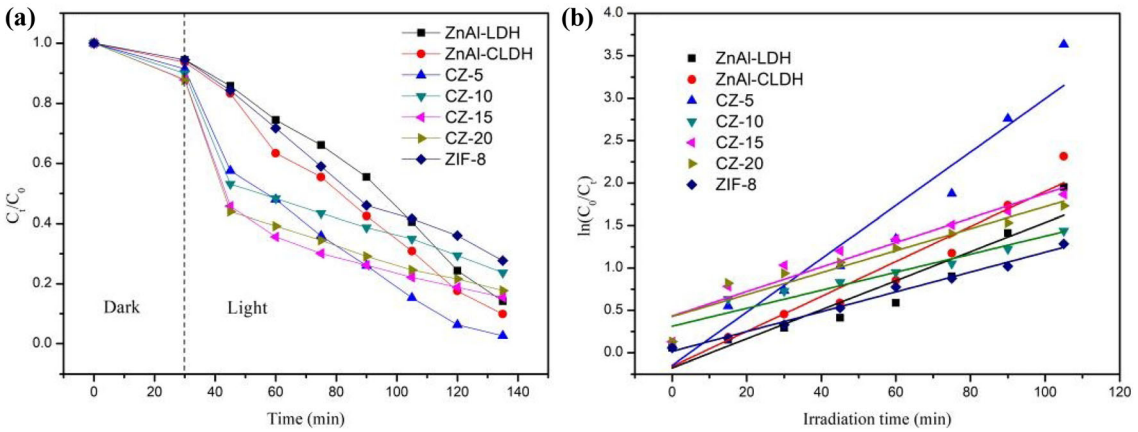

Fig. 7 **a** Photocatalytic degradation of MB with as-prepared catalysts; **b** The pseudo-first-order kinetics model of samples under irradiation

advantage of the combination of these two materials. It is worth noting that ZnAl-CLDH exhibits higher photocatalytic activity (90.12%) than that of ZIF-8 (72.34%). As shown in the Fig. 7a, after adding ZIF-8, the adsorption rates of the composites in the first 30 min under dark conditions have been significantly improved. At the loading of 10%, 15% and 20%, the ZnAl-CLDH/ZIF-8 composites degraded MB solution by 64.45%, 84.54% and 81.70%, respectively, which demonstrated the importance of the dosage of doped ZIF-8.

It is significant to obtain the apparent rate constant k to further investigate the photocatalytic activities quantitatively. Therefore, a pseudo-first-order model (Eq. 1) should be used to analyze the experimental data cause the low MB concentration and the experimental data corresponded to the Langmuir–Hinshelwood model [32, 38, 39, 41].

$$\ln\left(C_0/C_t\right) = kt \quad (1)$$

In this equation, k stands for the apparent pseudo-first-order rate constant (min^{-1}), and t is the time (min). C_0 and C_t represent the initial concentration and the real-time concentration respectively. Fig. 7b demonstrates the dynamics analysis results by the relationship of ln (C_0/C_t) against t when the R^2 value of each line is closed to 1. Obviously, CZ-5 shows the highest k (0.03143 min^{-1}) among these as-prepared samples, proving the composite of ZnAl-CLDH coupled with 5% ZIF-8 has the fastest photodegradation rate of MB. In contrast, the k values of pure ZnAl-CLDH and ZIF-8 are 0.0206 min^{-1} and 0.0117 min^{-1}, which are approximately two-thirds and one-third of that of CZ-5 respectively. All of the parameters for the removal of MB solution were shown in Table 3. These results further confirm the enhanced photocatalytic activity of the combination of ZnAl-CLDH and ZIF-8.

3.2.2 *Photocatalytic stability*

The reusability is an important factor in choosing ZnAl-CLDH/ZIF-8 composite in practical applications. Therefore, five successive photodegration processes were implemented under the same conditions. After each process run, the reclaimed catalyst was restored by washed, filtrated and dried. The results can be seen in Fig. 8 that the MB photodegradation activity of the photocatalyst retain 92.59% after five cycles. The results exhibit the ZnAl-CLDH/ZIF-8 composite can be used as a promising catalyst with remarkable stability.

3.2.3 *Radical scavenging*

In order to explore the main active species in the degradation process, the radical scavenging experiment was carried out. During the test, the activities of hydroxyl radicals (·OH), photogenerated holes (h^+), and superoxide radical anions ($\cdot O_2^-$) were restricted by Isopropyl alcohol (IPA), Ethylene diamine tetraacetic acid (EDTA), and 1,4-benzoquinone (BQ), respectively [3, 6, 42]. As shown in Fig. 9, the addition of IPA and EDTA has a significant effect on the degradation rate, which drops to 14.56% and 6.76% respectively. On the contrary, after adding BQ, the degradation efficiency is still above 90%. The results

Table 3 Pseudo-first-order parameters for the removal of MB solution

Catalyst	(ln $C_t/C_0 = -kt$, pseudo-first-order reaction)			
	k	R^2	Standard error	DE_{135min} (%)
ZnAl-LDH	0.01712	0.90020	0.00236	85.80
ZnAl-CLDH	0.0206	0.92498	0.0022	90.12
CZ-5	0.03143	0.92152	0.00345	97.35
CZ-10	0.01062	0.91418	0.00122	76.30
CZ-15	0.01442	0.90986	0.0017	84.53
CZ-20	0.01295	0.91659	0.00165	82.30
ZIF-8	0.0117	0.99002	0.000443	72.34

of the radical scavenging experiment suggesting the major components in the progress of the reaction are ·OH and h^+.

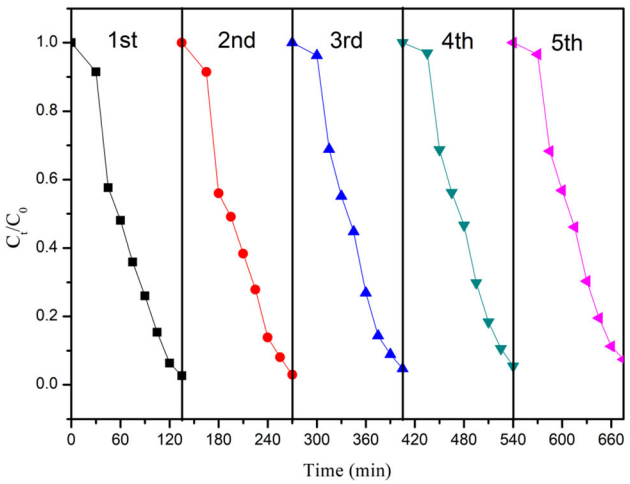

Fig. 8 Recycled runs for photodegradation of MB with the CZ-5 composite

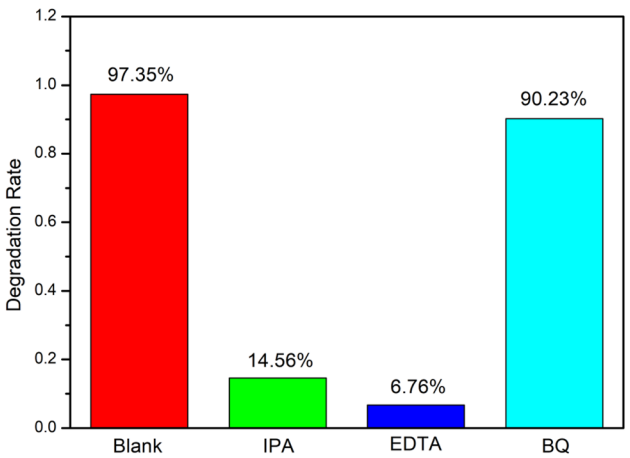

Fig. 9 The effects of different scavengers on the degradation efficiency of MB with CZ-5

3.2.4 *Photocatalytic mechanism*

According to the results of the radical trapping experiment, $\cdot O_2^-$, ·OH and h^+ are significant in the phtocatalytic process, especially ·OH and h^+. As shown in Fig. 10, a logical mechanism of MB degradation over ZnAl-CLDH/ZIF-8 composites could be composed under the light illumination. Based on previous reports, the Conduction band (CB) potentials of ZnAl-CLDH and ZIF-8 are − 0.31 eV and − 0.86 eV (vs. NHE), respectively [6, 13, 30, 43, 44]. The Conduction band (CB) and the valence band (VB) edge potentials can be analyzed by the formula: $E_{CB} = E_{VB} - E_g$. According to the UV–vis DRS results, the Valence band (VB) potentials of them are 2.11 eV and 3.32 eV (vs. NHE), respectively. Therefore, the I-scheme heterostructure is formed between ZnAl-CLDH and ZIF-8 [45–47]. Due to the CB of ZIF-8 is more negative than that of ZnAl-CLDH, the photoelectrons on ZIF-8 will transfer to ZnAl-CLDH. Moreover, $E_0(O_2/O_2^-)$ (− 0.33 eV vs. NHE) is more negative than the CB of ZnAl-CLDH but more positive than that of ZIF-8, thus $\cdot O_2^-$ can be produced on ZIF-8 but not on ZnAl-CLDH. Therefore, there are not enough electrons to generate $\cdot O_2^-$ so that the role of $\cdot O_2^-$ in the degradation reaction is not so significant, which is consistent with the results of the radical scavenging experiment. Meanwhile, the photogenerated holes will also shift from ZIF-8 to ZnAl-CLDH because the VB edge potential of ZIF-8 is more positive than that of ZnAl-CLDH. Due to $E_0(H_2O/OH)$ is about 1.9 eV, ·OH can be generated massively on ZnAl-CLDH, corresponding to the results of radical trapping. In general, only the MB on the surface can be photodegraded because these active substances are difficult to dispense in solution. Therefore, by compounding ZIF-8 with a large specific surface area, the adsorption capacity of the

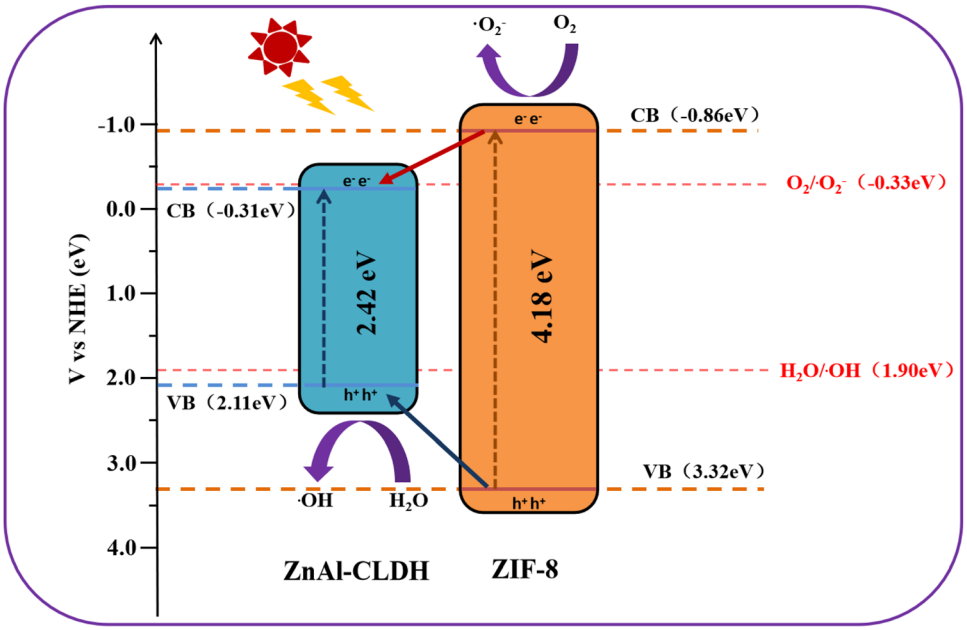

Fig. 10 Schematic diagram of photocatalytic mechanism in aqueous solution for the ZnAl-CLDH/ZIF-8

catalyst can be significantly increased, thereby enhancing the photocatalytic activity. In addition, the degradation process can be expressed by the equations below.

$$\mathrm{ZnAl-CLDH/ZIF-8} + hv \rightarrow \mathrm{ZnAl-CLDH}\ (h^{+}_{VB}) + \mathrm{ZIF-8}\ (e^{-}_{CB}) \quad (2)$$

$$\mathrm{ZIF\text{-}8}\ (e^{-}_{CB}) + O_2 \rightarrow \cdot O_2^{-} + \mathrm{ZIF\text{-}8} \quad (3)$$

$$\mathrm{ZnAl\text{-}CLDH}\ (h^{+}_{VB}) + OH^{-} \rightarrow \cdot OH + \mathrm{ZnAl\text{-}CLDH} \quad (4)$$

$$\cdot O_2^{-} + \mathrm{MB} \rightarrow \mathrm{Degradation\ products} \quad (5)$$

$$\cdot OH + \mathrm{MB} \rightarrow \mathrm{Degradation\ products} \quad (6)$$

4 Conclusion

In this work, an effective strategy to synthesize the ZnAl-CLDH/ZIF-8 composites was supplied. The statuses and morphologies were proved by several characterization methods such as XRD, SEM, XPS and UV–vis DRS. The heterostructure was formed to restrict the recombination of photon-generated carriers. Through the degradation of target pollutants (MB), the ZnAl-CLDH/ZIF-8 composites with 5% ZIF-8 exhibit optimal photocatalytic performance (97.35%) than pure ZnAl-CLDH and ZIF-8. After five cycle runs, the photodegradation efficiency is still remain 92.59%, proving the remarkable stability and reusability of the composite. Furthermore, ·OH and h^+ are the main reactive components in the photodegradation process by the radical scavenging experiment. Finally, a possible mechanism was proposed to suggest a new idea for practical application.

Acknowledgements

This work was financially supported by National Natural Science Foundation of China (Grant No. 21776319), the Fundamental Research Funds for the Central South University (Grant No. 2020zzts389) and the Funds for the Hunan Graduate Education Innovation Project and Professional Ability Upgrading Project (Grant No. CX20200162).

Author contributions

YW: Methodology, Investigation, Writing—original draft. YZ: Writing—review and editing. GZ: Data curation. SL: Characterization. JH: Formal analysis. XL: Visualization. ZX: Investigation. HZ: Supervision, Resources. FJ: Conceptualization, Resources, Project administration.

Funding

This work was financially supported by National Natural Science Foundation of China (Grant No. 21776319), the Fundamental Research Funds for the Central South University (Grant No. 2020zzts389) and the Funds for the Hunan Graduate Education Innovation Project and Professional Ability Upgrading Project (Grant No. CX20200162).

Data availability

The data and material were available.

Code availability

Not applicable.

Declarations

Conflict of interest The authors declare that they have no known competing financial interests or personal relationships that could have appeared to influence the work reported in this paper.

References

1. J. Wang, R.S. Chen, L. Xiang, S. Komarneni, Synthesis, properties and applications of ZnO nanomaterials with oxygen vacancies: a review. Ceram. Int. **44**, 7357–7377 (2018)
2. G.Q. Zhao, D. Zhang, Y.L. Huang, J.G. Yu, X.Y. Jiang, F.P. Jiao, Highly efficient degradation of 2-chlorophenol and methylene blue with $Rb_{0.27}WO_3$/NiFe-CLDH composites under visible light irradiation. Adv. Powder. Technol. **26**, 2491–2500 (2018)
3. J.F. Ma, J.F. Ding, L.M. Yu, L.Y. Li, Y. Kong, S. Komarneni, BiOCl dispersed on NiFe-LDH leads to enhanced photodegradation of Rhodamine B dye. Appl. Clay. Sci. **109–110**, 76–82 (2015)
4. X. Zhu, L. Zhu, H. Li, J.W. Xue, C. Ma, Y.Y. Yin, X.R. Qiao, D.F. Sun, Q.Z. Xue, Multifunctional charged hydrogel nanofibrous membranes for metal ions contained emulsified oily wastewater purification. J. Membr. Sci. **621**, 118950 (2021)
5. M. Shao, A.W. Wang, H.J. Cui, Z.Y. Liu, Y.H. Xu, Z.Y. Li, S. Xu, Fabrication of $ZnFe_2O_4$ decorated CdS nanosphere composites with excellent visible light photocatalytic activity. J. Mater. Sci. Mater. El. **31**, 1472–1482 (2020)
6. F. Ahmadi, M. Rahimi-Nasrabadi, A. Fosooni, M. Daneshmand, Synthesis and application of $CoWO_4$ nanoparticles for degradation of methyl orange. J. Mater. Sci. Mater. El. **27**, 9514–9519 (2016)
7. Y. Liu, G. Wang, W.N. Yang, J. Yang, J. Li, Biotemplated synthesis of hierarchically porous ZnAl-CLDH/$FeWO_4$ for effective removal of dyes from water. Water. Air. Soil. Poll. **230**, 89 (2019)
8. G.Q. Zhao, J. Zou, X.Q. Chen, J.G. Yu, F.P. Jiao, Layered double hydroxides materials for photo (electro-) catalytic applications. Chem. Eng. J. **397**, 125407 (2020)
9. G.H. Zhang, X.Q. Zhang, Y. Meng, G.X. Pan, Z.M. Ni, S.J. Xia, Layered double hydroxides-based photocatalysts and visible-light driven photodegradation of organic pollutants: a review-science direct. Chem. Eng. J. **392**, 123684 (2020)
10. L. Mohapatra, K. Parida, A review on the recent progress, challenges and perspective of layered double hydroxides as promising photocatalysts. J. Mater. Chem. A **4**, 10744–10766 (2016)
11. X.H. Luo, S. Yuan, X.Y. Pan, C.X. Zhang, S. Du, Y.L. Liu, Synthesis and enhanced corrosion protection performance of reduced graphene oxide nanosheet/ZnAl layered double hydroxide composite films by hydrothermal continuous flow method. ACS Appl. Mater. Inter. **9**, 18263–18275 (2017)
12. Y.F. Zhao, X.D. Jia, G.I.N. Waterhouse, L.Z. Wu, C.H. Tung, D. O'Hare, T.R. Zhang, Layered double hydroxide nanostructured photocatalysts for renewable energy production. Adv. Energy. Mater. **6**, 1501974 (2016)
13. D.Y. Yu, S.G. Wen, J.X. Yang, J.H. Wang, Y. Chen, J. Luo, Y.T. Wu, RGO modified ZnAl-LDH as epoxy nanostructure filler: a novel synthetic approach to anticorrosive waterborne coating. Surf. Coat. Tech. **326**, 207–215 (2017)
14. X. Wu, D. Zhang, F.P. Jiao, S. Wang, Visible-light-driven photodegradation of methyl orange using Cu_2O/ZnAl calcined layered double hydroxides as photocatalysts. Colloid Surf. A **508**, 110–116 (2016)
15. G.Q. Zhao, C.F. Li, X. Wu, J.G. Yu, X.Y. Jiang, W.J.H. Hu, F.P. Jiao, Reduced graphene oxide modifed NiFe-calcinated layered double hydroxides for enhanced photocatalytic removal of methylene blue. Appl. Clay. Sci. **434**, 251–259 (2018)
16. X. Liu, J. Luo, Y. Zhu, Y. Yang, S. Yang, Removal of methylene blue from aqueous solutions by an adsorbent based on metal-organic framework and polyoxometalate. J. Alloy. Compd. **648**, 986–993 (2015)
17. K.M. Choi, K. Na, G.A. Somorjai, O.M. Yaghi, Chemical environment control and enhanced catalytic performance of platinum nanoparticles embedded in nanocrystalline metal-organic frameworks. J. Am. Chem. Soc. **137**, 7810–7816 (2015)

18. Q. Liang, M. Zhang, Z. Zhang, C. Liu, S. Xu, Z. Li, Zinc phthalocyanine coupled with UIO-66 (NH_2) via a facile condensation process for enhanced visiblelight-driven photocatalysis. J. Alloy. Compd. **690**, 123–130 (2017)
19. L.Y. Chen, Y. Peng, H. Wang, Z.Z. Gu, C.Y. Duan, Synthesis of Au@ZIF-8 single- or multi-core-shell structures for photocatalysis. Chem. Commun. **50**, 8651–8654 (2014)
20. Y.H. Ding, X.L. Zhang, N. Zhang, J.Y. Zhang, R. Zhang, Y.F. Liu, Y.Z. Fang, A visible-light driven Bi_2S_3@ZIF-8 core-shell heterostructure and synergistic photocatalysis mechanism. Dalton. Trans. **47**, 684–692 (2018)
21. H. Li, L. Zhu, X. Zhu, M. Chao, J.W. Xue, D.F. Sun, F.J. Xia, Q.Z. Xue, Dual-functional membrane decorated with flower-like metal–organic frameworks for highly efficient removal of insoluble emulsified oils and soluble dyes. J. Hazard. Mater. **408**, 124444 (2021)
22. L.H. Wee, N. Janssens, S.P. Sree, C. Wiktor, E. Gobechiya, R.A. Fischer, C.E. Kirschhock, J.A. Martens, Local transformation of ZIF-8 powders and coatings into ZnO nanorods for photocatalytic application. Nanoscale **6**, 2056–2060 (2014)
23. P.F. Zhu, X.H. Yin, X.H. Gao, G.H. Dong, J.K. Xu, C.Y. Wang, Enhanced photocatalytic NO removal and toxic NO_2 production inhibition over ZIF-8-derived ZnO nanoparticles with controllable amount of oxygen vacancies. Chinese J. Catal. **42**, 175–183 (2021)
24. J. Liu, J. He, L. Wang, R. Li, P. Chen, X. Rao, L. Deng, L. Rong, J. Lei, NiO-PTA supported on ZIF-8 as a highly effective catalyst for hydrocracking of Jatropha oil. Sci. Rep. UK **6**, 23667 (2016)
25. X.B. Wang, J. Liu, S. Leong, X.C. Lin, J. Wei, B. Kong, Y.F. Xu, Z. Low, J.F. Yao, H.T. Wang, Rapid construction of ZnO@ZIF-8 heterostructures with size-selective photocatalysis properties. ACS Appl. Mater. Inter. **8**, 9080–9087 (2016)
26. J.X. Liu, R. Li, Y.F. Wang, Y.W. Wang, X.C. Zhang, C.M. Fan, The active roles of ZIF-8 on the enhanced visible photocatalytic activity of Ag/AgCl: generation of superoxide radical and adsorption. J. Alloy. Compd. **693**, 543–549 (2017)
27. G. Mendoza-Damian, F. Tzompantzi, A. Mantilla, R. Pérez-Hernández, A. Hernández-Gordillo, Improved photocatalytic activity of SnO_2-ZnAl LDH prepared by one step Sn^{4+} incorporation. Appl. Clay. Sci. **121**, 127–136 (2016)
28. Z.Y. Zhang, D.J. Sun, G.R. Li, B. Zhang, B. Zhang, S.M. Qiu, Y.J. Li, T. Wu, Calcined products of Mg-Al layered double hydroxides/single-walled carbon nanotubes nanocomposites for expeditious removal of phenol and 4-chlorophenol from aqueous solutions. Colloid Surf. A **565**, 143–153 (2019)
29. J.S. Liu, J.X. Chen, Z.Y. Wu, K.J. Zhu, J. Wang, Z.Q. Li, G.A. Tai, X.Q. Liu, S.L. Lu, Enhanced visible-light photocatalytic performances of ZnO through loading AgI and coupling piezo-photocatalysis. J. Alloy. Compd. **852**, 156848 (2021)
30. A. Khataee, R.D.C. Soltani, Y. Hanifehpour, M. Safarpour, H.G. Ranjbar, S.W. Joo, Synthesis and characterization of dysprosium-doped ZnO nanoparticles for photocatalysis of a textile dye under visible light irradiation. Ind. Eng. Chem. Res. **53**, 1924–1932 (2014)
31. A. Karimi, A. Khataee, M. Safarpour, V. Vatanpour, Development of mixed matrix ZIF-8/polyvinylidene fluoride membrane with improved performance in solvent resistant nanofiltration. Sep. Purif. Technol. **237**, 116358 (2020)
32. Y.M. He, L. Zeng, Z. Feng, Q.L. Zhang, X.Y. Zhao, S.F. Ge, X. Hu, H.J. Lin, Preparation, characterization, and photocatalytic activity of novel AgBr/ZIF-8 composites for water purification. Adv. Powder. Technol. **31**, 439–447 (2020)
33. Y. Liu, L. Deng, J.P. Sheng, F.Y. Tang, K. Zeng, L.Q. Wang, K.X. Liang, H. Hu, Y.N. Liu, Photostable core-shell CdS/ZIF-8 composite for enhanced photocatalytic reduction of CO_2. Appl. Clay. Sci. **498**, 143899 (2019)
34. B.H. Ren, Y.N. Chen, Y.Q. Li, W.J. Li, S.Y. Gao, H.F. Li, R. Cao, Rational design of metallic anti-corrosion coatings based on zinc gluconate@ZIF-8. Chem. Eng. J. **384**, 123389 (2019)
35. S.B. Wang, X.C. Wang, Photocatalytic CO_2 reduction by CdS promoted with a zeolitic imidazolate framework. Appl. Catal. B-Environ. **162**, 494–500 (2015)
36. W.H. Fei, Y. Song, N.J. Li, D.Y. Chen, Q.F. Xu, H. Li, J.H. He, J.M. Lu, Fabrication of visible-light-active ZnO/ZnFe-LDH heterojunction on Ni foam for pollutants removal with enhanced photoelectrocatalytic performance. Sol. Energy **188**, 593–602 (2019)
37. G.L. Di, Z.L. Zhu, Q.H. Huang, H. Zhang, J.Y. Zhu, Y.L. Qiu, D.Q. Yin, J.F. Zhao, Targeted modulation of g-C_3N_4 photocatalytic performance for pharmaceutical pollutants in water using ZnFe-LDH derived mixed metal oxides: structure-activity and mechanism. Sci. Total. Environ. **650**, 1112–1121 (2019)
38. X.R. Wang, P.X. Wu, Z.J. Huang, N.W. Zhu, J.H. Wu, P. Li, Z. Dang, Solar photocatalytic degradation of methylene blue by mixed metal oxide catalysts derived from ZnAlTi layered double hydroxides. Appl. Clay. Sci. **95**, 95–103 (2014)
39. Y.F. Zhan, J.W. Lan, J.J. Shang, L. Yang, X.M. Guan, W.X. Li, S.Q. Chen, Y. Qi, S.J. Lin, Durable ZIF-8/Ag/AgCl/TiO_2 decorated PAN nanofibers with high visible light photocatalytic and antibacterial activities for degradation of dyes. J. Alloy. Compd. **822**, 153579 (2020)
40. F.A. Beni, A. Gholami, A. Ayati, M.N. Shahrak, M. Sillanpaa, UV-switchable phosphotungstic acid sandwiched between ZIF-8 and Au nanoparticles to improve simultaneous adsorption and UV light photocatalysis toward tetracycline

degradation. Microporous. Mesoporous. Mater. **303**, 110275 (2020)
41. X.M. Guan, S.J. Lin, J.W. Lan, J.J. Shang, W.X. Li, Y.F. Zhan, H.Y. Xiao, Q.S. Song, Fabrication of Ag/AgCl/ZIF-8/TiO_2 decorated cotton fabric as a highly efficient photocatalyst for degradation of organic dyes under visible light. Cellulose **26**, 7437–7450 (2019)
42. J.B. Zhou, W. Liu, W.Q. Cai, The synergistic effect of Ag/AgCl@ZIF-8 modified g-C_3N_4 composite and peroxymonosulfate for the enhanced visible-light photocatalytic degradation of levofloxacin. Sci. Total. Environ. **696**, 133962 (2019)
43. M.Q. Hua, H. Lou, X.L. Yan, X.Y. Hua, R. Feng, M. Zhou, In-situ fabrication of ZIF-8 decorated layered double oxides for adsorption and photocatalytic degradation of methylene blue. Microporous. Mesoporous. Mater. **271**, 68–72 (2018)
44. X.Y. Yuan, W.Y. Li, Graphitic-C_3N_4 modified ZnAl-layered double hydroxides for enhanced photocatalytic removal of organic dye. Appl. Clay. Sci. **138**, 107–113 (2017)
45. Y.P. Xie, Y. Yang, G. Wang, G. Liu, Oxygen vacancies promoted interfacial charge carrier transfer of CdS/ZnO heterostructure for photocatalytic hydrogen generation. J. Colloid. Interf. Sci. **503**, 198–204 (2017)
46. L. Xu, Q.Q. Jiang, Z.H. Xiao, X.Y. Li, J. Huo, S.Y. Wang, L.M. Dai, Plasma-engraved Co_3O_4 nanosheets with oxygen vacancies and high surface area for the oxygen evolution reaction. Angew. Chem. Int. Ed. **55**, 5277–5281 (2016)
47. J.X. Low, J. Yu, M. Jaroniec, S. Wageh, A.A. Al-Ghamdi, Heterojunction photocatalysts. Adv. Mater. **29**, 1601694 (2017)